

# Microscopic study of the $^{132,124}\text{Sn}+^{96}\text{Zr}$ reactions: dynamic excitation energy, energy-dependent heavy-ion potential, and capture cross section

V.E. Oberacker,<sup>1</sup> A.S. Umar,<sup>1</sup> J.A. Maruhn,<sup>2</sup> and P.-G. Reinhard<sup>3</sup>

<sup>1</sup>*Department of Physics and Astronomy, Vanderbilt University, Nashville, Tennessee 37235, USA*

<sup>2</sup>*Institut für Theoretische Physik, Goethe-Universität, D-60438 Frankfurt am Main, Germany*

<sup>3</sup>*Institut für Theoretische Physik, Universität Erlangen, D-91054 Erlangen, Germany*

(Dated: November 5, 2018)

We study reactions between neutron-rich  $^{132}\text{Sn}$  nucleus and  $^{96}\text{Zr}$  within a dynamic microscopic theory at energies in the vicinity of the ion-ion potential barrier peak, and we compare the properties to those of the stable system  $^{124}\text{Sn}+^{96}\text{Zr}$ . The calculations are carried out on a three-dimensional lattice using the density-constrained Time-Dependent Hartree-Fock method. In particular, we calculate the dynamic excitation energy  $E^*(t)$  and the quadrupole moment of the dinuclear system,  $Q_{20}(t)$ , during the initial stages of the heavy-ion collision. Capture cross sections for the two reactions are analyzed in terms of dynamic effects and a comparison with recently measured data is given.

PACS numbers: 21.60.-n, 21.60.Jz

## I. INTRODUCTION

Heavy-ion reactions at radioactive ion beam (RIB) facilities allow us to form new exotic neutron-rich nuclei and to study their physical properties. Examples include experiments with neutron-rich  $^{132}\text{Sn}$  beams on targets of  $^{64}\text{Ni}$  [1, 2] and of  $^{96}\text{Zr}$  [3]. Another experimental frontier is the synthesis of superheavy nuclei in cold fusion reactions involving spherical closed-shell  $^{208}\text{Pb}$  targets [4] and in hot fusion reactions with deformed actinide nuclei [5]. These experiments present numerous challenges for a theoretical description, in particular for dynamic microscopic theories.

At relatively large impact parameters, heavy-ion reactions are dominated by deep inelastic collisions in which the nuclei make only brief contact. The reaction products have mass and charge similar to projectile and target, but the energy may be strongly damped. At smaller impact parameters, an intermediate dinuclear system is formed. Entrance-channel heavy-ion potentials have been calculated in various models, including the macroscopic-microscopic method with five shape parameters [6], and the energy density functional method with extended Thomas-Fermi approximation [7]. Furthermore, dynamical models [8–10] show that if the dinuclear system is able to move inside the saddle point, capture occurs which may lead to the formation of a compound nucleus with compact shape. During capture the energy of relative motion of the ions gets converted into intrinsic excitation energy  $E^*(t)$ . If a compound nucleus is formed it will subsequently decay either by particle evaporation or by fission. On the other hand, if the dinuclear system separates before crossing the saddle point, the reaction process is called quasifission. In this case, the shape of the dinuclear system is very elongated (large quadrupole moment). Experimentally, it is possible to separate fusion-fission from quasifission by measuring the angular anisotropy of the fragments. In the

collision of very heavy ions such as  $^{132}\text{Sn}+^{96}\text{Zr}$  considered in this paper, studies of fusion reactions are complicated by the competition with quasifission and fusion-fission events which hinder the formation of evaporation residues.

The time-dependent Hartree-Fock (TDHF) theory provides a useful foundation for a fully microscopic many-body theory of heavy-ion collisions in the vicinity of the Coulomb barrier [11, 12]. Partly because of the recent breakthroughs in microprocessor technology, it has become feasible to perform TDHF calculations on a three-dimensional (3D) Cartesian grid with no symmetry restrictions and with much more accurate numerical methods. At the same time the quality of effective interactions has also been substantially improved [13, 14]. These developments allow for the testing of the time-dependent mean-field approach to nuclear reactions without any numerical uncertainties [15–18]. The TDHF code used in these calculations utilizes the full Skyrme interaction, including all of the time-odd terms in the mean field Hamiltonian [15, 19].

During the past several years, we have developed the density-constrained (DC) TDHF method (DC-TDHF) for calculating heavy-ion potentials [20]. We have applied this method to calculate fusion cross sections above and below the barrier for a number of systems: The first application was for the  $^{132}\text{Sn}+^{64}\text{Ni}$  [21, 22] system. The fusion cross section at the lowest projectile energy has been re-measured [2] and now agrees remarkably well with our calculations. We have also performed calculations for  $^{64}\text{Ni}+^{64}\text{Ni}$  [23] and for  $^{16}\text{O}+^{208}\text{Pb}$  [24]. In all these cases, we have found very good agreement between the measured fusion cross sections and the DC-TDHF results. Very recently, we have carried out a microscopic dynamical study of the astrophysical triple- $\alpha$  reaction to form a resonant state of  $^{12}\text{C}$  [25] and a study similar to the one presented here for reactions involving superheavy formations [26], using the same approach.

In the present paper, we study reactions between

the neutron-rich  $^{132}\text{Sn}$  nucleus and  $^{96}\text{Zr}$  at energies in the vicinity of the ion-ion potential barrier peak, and we compare observables to those of the stable system  $^{124}\text{Sn}+^{96}\text{Zr}$ . The dynamic microscopic calculations are carried out on a 3D Cartesian lattice using both unrestricted TDHF and DC-TDHF methods. This is by far the heaviest neutron-rich system we have investigated so far, and the microscopic numerical calculations with the added DC are computationally very intensive.

This paper is organized as follows: in Section II we summarize the Formalism (DC-TDHF, dynamic excitation energy, capture cross section). In Section III numerical results are presented. In particular, we show contour plots of the mass density of the dinuclear system and discuss the dynamic quadrupole moment  $Q_{20}(t)$  during the initial stages of the collision. We also calculate the heavy-ion interaction potential  $V(R)$  and demonstrate that in these very heavy systems the barrier height and width increase dramatically with increasing beam energy. Interaction barrier heights and positions are also deduced from unrestricted TDHF runs. We examine the dynamic excitation energy  $E^*(t)$  during the initial stages of the collision and compare it to the excitation energy of the compound nucleus in its ground state,  $E^* = E_{c.m.} + Q_{gg}$ . Finally, capture cross sections for the two reactions are analyzed in terms of dynamic effects, and a comparison with recently measured capture-fission data [3] is given. The conclusions are presented in Section IV.

## II. FORMALISM: DC-TDHF METHOD, DYNAMIC EXCITATION ENERGY, CAPTURE

Recently, we have developed a method to extract ion-ion interaction potentials directly from the TDHF time-evolution of the nuclear system. In our DC-TDHF approach [20], the TDHF time-evolution takes place with no restrictions. At certain times during the evolution the instantaneous density is used to perform a static Hartree-Fock minimization while holding the total proton and neutron density of the dinuclear system constrained to be the instantaneous TDHF density. This provides us with the TDHF dynamical path in relation to the multi-dimensional static energy surface of the combined nuclear system. In the DC-TDHF method the ion-ion interaction potential is given by

$$V(R) = E_{\text{DC}}(R) - E_{A_1} - E_{A_2} , \quad (1)$$

where  $E_{\text{DC}}$  is the DC energy at the instantaneous separation  $R(t)$ , while  $E_{A_1}$  and  $E_{A_2}$  are the binding energies of the two nuclei obtained with the same effective interaction. The interaction potentials calculated with the DC-TDHF method incorporate all of the dynamical entrance channel effects such as neck formation, particle exchange, internal excitations, and deformation effects. While the outer part of the potential barrier is largely determined by the entrance channel properties, the inner part of the

potential barrier is strongly sensitive to dynamical effects such as particle transfer and neck formation.

For the calculation of the ion-ion separation distance  $R$  we use a hybrid method as described in Ref. [24]. At large distances where a still visible neck allows us to identify two fragments we compute it as distance of the center of mass of the ions. For more compact configurations, we compute  $R$  from the mass quadrupole moment  $Q_{20}$  as  $R = r_0 \sqrt{|Q_{20}|}$  where  $r_0$  is a scale factor to connect the definition smoothly to the large-distance region.

In heavy-ion reactions, the total capture cross section consists of the following terms [3]:

$$\sigma_{\text{capt}} = \sigma_{\text{ER}} + \sigma_{\text{QF}} + \sigma_{\text{FF}} , \quad (2)$$

where  $\sigma_{\text{ER}}$ ,  $\sigma_{\text{QF}}$ ,  $\sigma_{\text{FF}}$  denote the evaporation residue cross section, the quasifission cross section, and the fusion-fission cross section. In the reaction of light and medium-heavy ions, the fission barriers of the pre-compound system are so high that fission contributions are negligible. In this case we have  $\sigma_{\text{capt}} \approx \sigma_{\text{ER}}$ . On the other hand, for the reaction of massive nuclei like  $^{132}\text{Sn}+^{96}\text{Zr}$ , the pre-compound system is an excited state of the actinide nucleus  $^{228}\text{Th}$  with a fission barrier of only about 6 MeV; thus we expect sizable fission contributions, and the evaporation residue cross section is expected to be rather small. The number of quasifission events increases dramatically with the product of the charge numbers  $Z_1 Z_2$  and with the orbital angular momentum  $\ell$  in the entrance channel. Another reason for the decreasing yield of ER formation is that a heated and rotating CN may fission (fusion-fission).

Ion-ion interaction potentials calculated using DC-TDHF correspond to the configuration attained during a particular TDHF collision. As mentioned above, for light and medium mass systems as well as heavier systems for which fusion is the dominant reaction channel, DC-TDHF gives the fusion barrier with an appreciable but relatively small energy dependence. On the other hand, for reactions involving massive systems fusion is not the dominant channel at barrier top energies. Instead the system sticks in some dinuclear configuration with possible break-up after exchanging a few nucleons. The long-time evolution to break-up is beyond the scope of TDHF due to the absence of quantum decay processes and transitions. As we increase the energy above the barrier this phenomenon gradually changes to the formation of a truly composite object. This is somewhat similar to the *extrapush* phenomenon discussed in phenomenological models. For this reason the energy dependence of the DC-TDHF ion-ion potential barriers for these systems is not just due to the dynamical effects for the same final configuration but actually represents different final configurations.

Theoretically, the calculation of the total capture cross section is similar to the calculation of the fusion cross

section

$$\sigma_{\text{capt}} = \frac{\pi}{k^2} \sum_{L=0}^{\infty} (2L+1) T_L, \quad (3)$$

with the understanding that the ion-ion interaction potential used in the calculations distinguishes the two events. In practice, the potential barrier penetrabilities  $T_L$  at  $E_{\text{c.m.}}$  energies below and above the barrier are obtained by numerical integration of the Schrödinger equation for the relative coordinate  $R$  using the well-established *Incoming Wave Boundary Condition* (IWBC) method [28, 29]. This Schrödinger equation contains the heavy-ion potential  $V(R)$  given in Eq. (1) and the centrifugal potential. In the IWBC calculations the summation over  $L$  in Eq. 3 is continued until the contribution becomes negligible to the total cross section. As we shall discuss below, we can also determine the maximum value of  $L$  by performing TDHF calculations for non-zero impact parameters. The optimal way to study the problem would be to perform DC-TDHF calculations for different  $L$  values, however for heavy systems the computational cost for doing this is very large. Finally, for the calculation of capture cross sections it is possible to use a coordinate dependent effective mass  $\mu(R)$  as described in Ref. [24]. The effect of using a coordinate dependent mass is to modify the inner part of the ion-ion potential, particularly at low subbarrier energies. For the energies studied here we have found this effect to be very small for capture cross sections.

Taking up the strategy proposed in [30], we have also developed a new microscopic approach for calculating dynamic excitation energies  $E^*(t)$  of systems formed during heavy-ion collisions [31]. For this purpose, we divide the conserved TDHF energy into a collective and intrinsic part, and we assume that the collective part is primarily determined by the density  $\rho(\mathbf{r}, t)$  and the current  $\mathbf{j}(\mathbf{r}, t)$ . Consequently, the excitation energy can be written in the form

$$E^*(t) = E_{\text{TDHF}} - E_{\text{coll}}(\rho(t), \mathbf{j}(t)), \quad (4)$$

where  $E_{\text{TDHF}}$  is the total energy of the dynamical system, which is a conserved quantity, and  $E_{\text{coll}}$  represents the collective energy of the system. The collective energy consists of two parts

$$E_{\text{coll}}(t) = E_{\text{kin}}(\rho(t), \mathbf{j}(t)) + E_{\text{DC}}(\rho(t)), \quad (5)$$

where  $E_{\text{kin}}$  represents the kinetic part and is given by

$$E_{\text{kin}}(\rho(t), \mathbf{j}(t)) = \frac{m}{2} \int d^3r \mathbf{j}^2(t)/\rho(t), \quad (6)$$

which is asymptotically equivalent to the kinetic energy of the relative motion,  $\frac{1}{2}\mu\dot{R}^2$ , where  $\mu$  is the reduced mass and  $R(t)$  is the ion-ion separation distance. The energy  $E_{\text{DC}}$  is the lowest-energy state of all possible TDHF states with the same density and is required to have zero

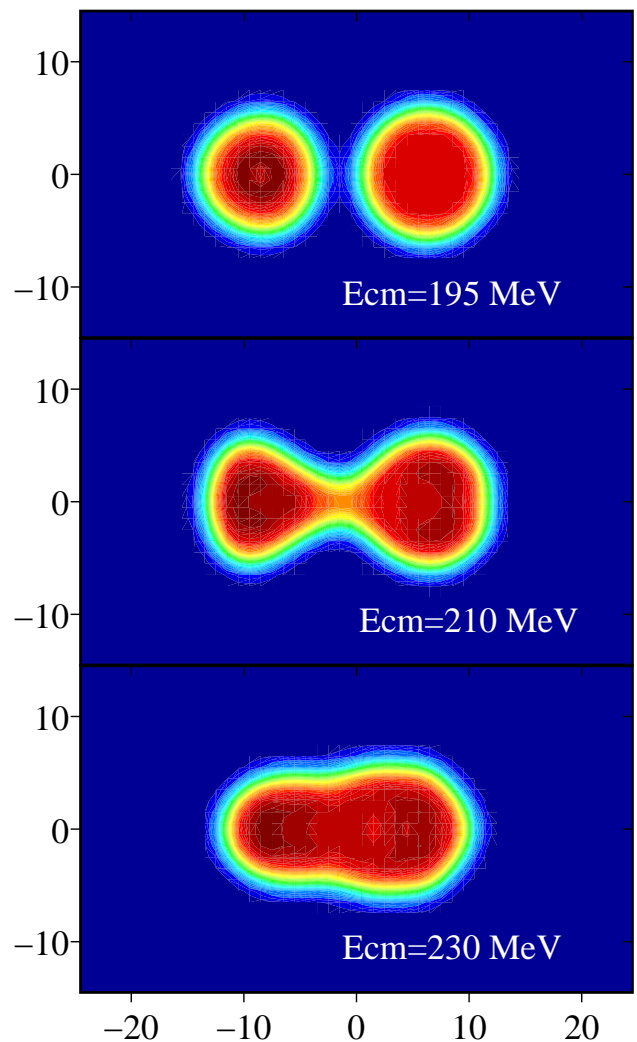


FIG. 1. (color online) TDHF calculations for  $^{132}\text{Sn}+^{96}\text{Zr}$ . Contour plots of the mass density at the distance of closest approach in a central collision, calculated at three different  $E_{\text{c.m.}}$  energies.

excitation energy. The dynamics of the ion-ion separation  $R(t)$  can be extracted from an unrestricted TDHF run. Using  $E^*(t)$  and  $R(t)$ , we can deduce the excitation energy as a function of the distance parameter,  $E^*(R)$ .

### III. RESULTS

The numerical calculations are carried out on a 3D Cartesian lattice using the Basis-Spline collocation method to represent derivative operators with high accuracy. For the  $^{132,124}\text{Sn}+^{96}\text{Zr}$  reactions studied here, the lattice spans 50 fm along the collision axis and 30–42 fm in the other two directions, depending on the impact parameter. The lattice spacing is 1.0 fm in all directions. We utilize the full Skyrme interaction (SLy4) [13] including all of the time-odd terms in the mean field Hamiltonian [15], without the c.m. correction as described in

Ref. [32]. The two nuclei are placed at an initial separation of 22 fm. First we generate highly accurate static HF wave functions for the two nuclei on the lattice, which are then boosted and time-propagated with a time step  $\Delta t = 0.4$  fm/c. The computation of the dynamic excitation energy and the heavy-ion potential is numerically very intensive, primarily due to the DC calculation. In a typical DC-TDHF run, we utilize a few thousand time steps, and the DC is applied every 20 time steps. To distinguish between deep-inelastic and capture reactions, we have also performed several unrestricted TDHF runs for the  $^{132}\text{Sn}+^{96}\text{Zr}$  system above the barrier. The numerical accuracy of the static binding energies and the deviation from the point Coulomb energy in the initial state of the collision dynamics is on the order of 50 – 200 keV. The accuracy of the DC calculations is commensurate with the accuracy of the static calculations.

### A. Dynamic quadrupole moment, Interaction Barrier, and Capture Barrier

In Fig. 1 we show contour plots of the mass density at the distance of closest approach in a central collision. These density plots reveal that at  $E_{\text{c.m.}} = 195$  MeV the nuclear surfaces barely touch; this energy corresponds to the interaction barrier. At  $E_{\text{c.m.}} = 210$  MeV we still notice a density configuration with two separate cores. Only at energies  $E_{\text{c.m.}} = 230$  MeV and above, a single-core composite system emerges, albeit with very large elongation. The large elongation of the composite system is readily apparent if one plots the intrinsic mass quadrupole moment

$$Q_{20}(t) = \sqrt{\frac{5}{16\pi}} \int d^3r \rho(\mathbf{r}, t) (2z^2 - x^2 - y^2) \quad (7)$$

as a function of time, see Fig. 2. Also shown, for comparison, is the static quadrupole moment of the compound nucleus  $^{228}\text{Th}$  which is more than three times smaller. Furthermore, the plot shows that central collisions at energies  $E_{\text{c.m.}} \geq 230$  MeV lead to capture while the nuclei bounce back from each other at  $E_{\text{c.m.}} = 220$  MeV and below (deep-inelastic collision).

As we have discussed earlier, for systems leading to superheavy formation the evaporation residue cross section is customarily represented in terms of the various phases of the reaction process as

$$\sigma_{\text{ER}} = \sigma_{\text{capture}} \cdot P_{\text{CN}} \cdot P_{\text{survival}}, \quad (8)$$

where  $\sigma_{\text{ER}}$  denotes the evaporation-residue cross section for the superheavy system,  $\sigma_{\text{capture}}$  is the capture cross section for the two-ions,  $P_{\text{CN}}$  is the probability of forming a compound nucleus, and  $P_{\text{survival}}$  is the probability that this compound system survives various breakup and fission events. The calculations presented here can only address the capture cross section for these systems since the subsequent reaction possibilities are beyond the scope

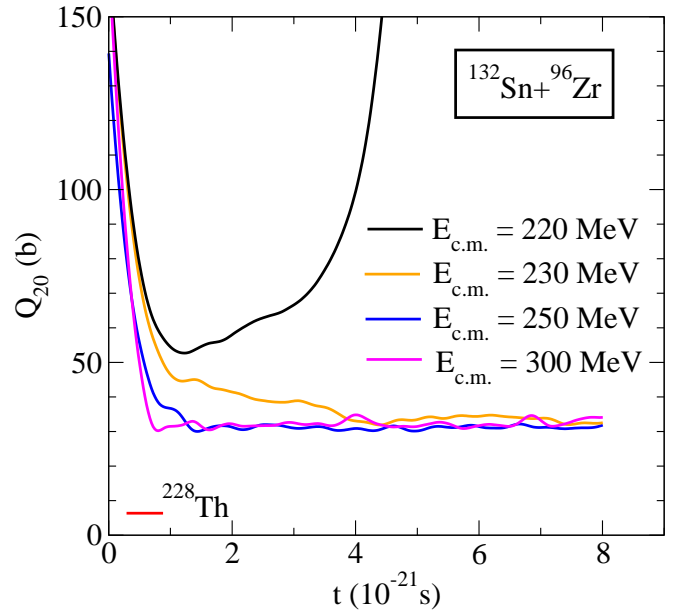


FIG. 2. (color online) Intrinsic mass quadrupole moment as a function of time.

of the TDHF theory. For most light systems, for which fusion is the dominant reaction result,  $\sigma_{\text{capture}}$  and  $\sigma_{\text{ER}}$  are essentially the same and equal to the fusion cross section,  $\sigma_{\text{fusion}}$ . For reactions involving superheavy formations we instead have

$$\sigma_{\text{capture}} = \sigma_{\text{QF}} + \sigma_{\text{FF}} + \sigma_{\text{ER}}, \quad (9)$$

where  $\sigma_{\text{QF}}$  and  $\sigma_{\text{FF}}$  denote the quasi-fission and fusion-fission cross sections, respectively. For these reactions the evaporation residue cross section,  $\sigma_{\text{ER}}$ , is very small and therefore the capture cross section is to a large extent equal to the sum of the two fission cross sections. Furthermore, the distinction between deep-inelastic reactions and quasi-fission is somewhat difficult and usually achieved by setting windows for fragment masses of  $A_f = A_{\text{CN}}/2 \pm 20$  and on their kinetic energy.

In Fig. 3 we show the ion-ion potential  $V(R)$  for a central collision of  $^{132}\text{Sn}+^{96}\text{Zr}$ , calculated at four different  $E_{\text{c.m.}}$  energies using the DC-TDHF method. The dotted part of the potential line calculated at  $E_{\text{c.m.}} = 220$  MeV corresponds to the outgoing trajectory (the nuclei bounce back in a deep-inelastic collision). Our results demonstrate that in these very heavy systems the barrier height and width increase dramatically with increasing energy  $E_{\text{c.m.}}$ . In fact, at higher energies the potential becomes almost flat. This is the first n-rich system in which we have observed this behavior. By contrast, DC-TDHF calculations for light ion systems such as  $^{16}\text{O}+^{16}\text{O}$  show almost no energy-dependence even if we increase  $E_{\text{c.m.}}$  by a factor of four [31]. Even in reactions between a light and a very heavy nucleus such as  $^{16}\text{O}+^{208}\text{Pb}$ , we see only a relatively small energy dependence of the barrier height and width [24]. For comparison, we have also plotted the phenomenological double-folding potential [33, 34] which

uses the ground state densities of the two nuclei and keeps them frozen. This potential is energy-independent and has been calculated using the M3Y effective NN interaction [35] and static 2-D HFB densities. We observe that the double-folding potential yields a potential barrier which is fairly similar to that of the DC-TDHF potential at  $E_{c.m.} = 230$  MeV; however, because of the frozen density approximation, the potential exhibits too much attraction at smaller distances. Another difference is that the ground state densities in the double folding method correspond to well bound nucleons. The TDHF densities, on the other hand, have much wider tails because they cover dynamically excited nucleons. This puts some part of the excitation energy into the DC-TDHF energy and hence into the ion-ion potential.

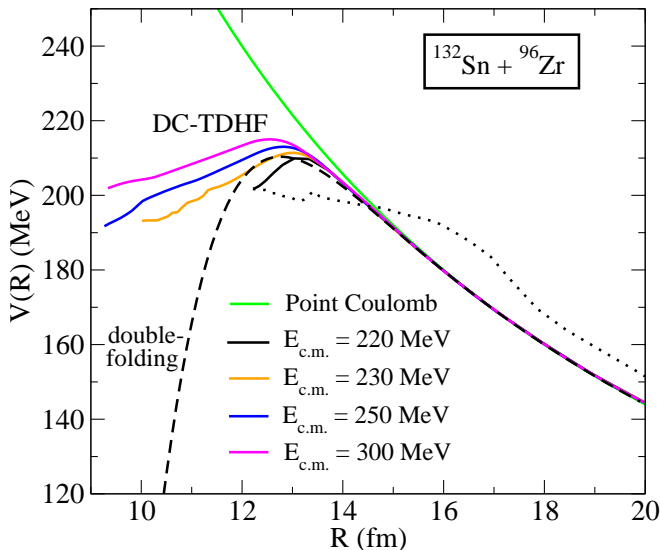


FIG. 3. (color online) DC-TDHF calculations for the neutron-rich system  $^{132}\text{Sn} + ^{96}\text{Zr}$ . The potential barriers  $V(R)$  at four  $E_{c.m.}$  energies are obtained using Eq. (1). Also shown is the point Coulomb potential. The phenomenological double-folding potential (dashed black curve) is given for comparison.

In Fig. 4 we show the ion-ion potential barriers in detail. A comparison is made between the neutron-rich system  $^{132}\text{Sn} + ^{96}\text{Zr}$  and the stable system  $^{124}\text{Sn} + ^{96}\text{Zr}$ . We find that the potential barriers of the neutron-rich system are systematically 1 – 2 MeV higher than those of the stable system. We emphasize again that only the potential barriers calculated at energies  $E_{c.m.} \geq 230$  MeV lead to a true composite system with overlapping cores (capture) while the potential barriers calculated at energies  $E_{c.m.} < 230$  MeV correspond to a dinuclear system where both nuclei maintain separate cores (deep-inelastic collisions).

The interaction barrier  $V_I$  is defined as the energy to bring the two colliding nuclei into contact [3]. This energy can be inferred from contour plots of the TDHF mass density at the distance of closest approach in a central collision, see Fig. 1. For  $^{132}\text{Sn} + ^{96}\text{Zr}$ , we find an interaction barrier height  $V_I = E_{c.m.} = 195$  MeV, and the cor-

responding distance of closest approach  $R_I = 14.77$  fm. In Table I we summarize the interaction barriers and ion-

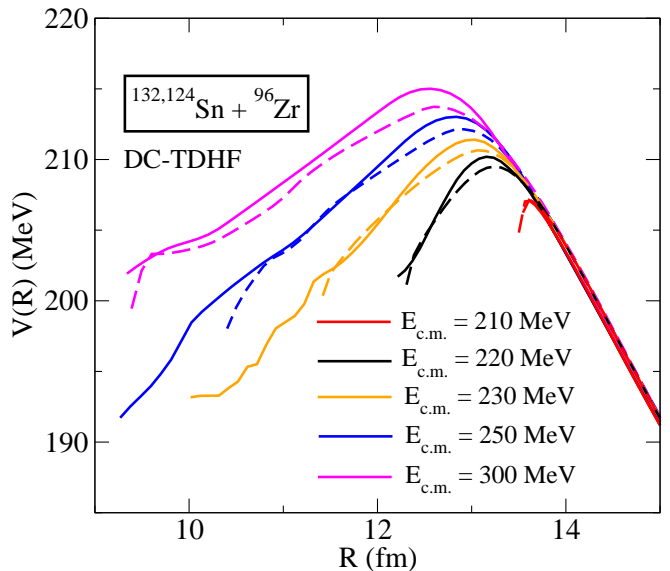


FIG. 4. (color online) Comparison of the heavy-ion barriers for the neutron-rich system  $^{132}\text{Sn} + ^{96}\text{Zr}$  (solid lines) and the stable system  $^{124}\text{Sn} + ^{96}\text{Zr}$  (dashed lines). The potential barriers are obtained with the DC-TDHF method at five  $E_{c.m.}$  energies.

ion potential barriers (capture barriers) for the two systems and their corresponding positions in  $R$ -space. While the DC-TDHF barriers are fairly similar, we observe large differences (9 MeV) in the interaction barriers of the two systems: the additional neutrons in  $^{132}\text{Sn}$  give rise to a larger attractive potential which causes the nuclei to snap together at lower energy. For TDHF collisions of

TABLE I. Interaction barrier heights  $V_I$  (energy to bring the two colliding nuclei into contact) and barrier positions  $R_I$  calculated with unrestricted TDHF at zero impact parameter. Also given are the energy-dependent ion-ion potential barrier heights  $V_B$  and positions  $R_B$  determined with the DC-TDHF method.

Reaction	$V_I$ (MeV)	$R_I$ (fm)	$V_B$ (MeV)	$R_B$ (fm)
$^{132}\text{Sn} + ^{96}\text{Zr}$	195	14.77	211.4 <sup>a</sup>	13.03 <sup>a</sup>
			215.0 <sup>b</sup>	12.56 <sup>b</sup>
$^{124}\text{Sn} + ^{96}\text{Zr}$	204	14.05	210.6 <sup>a</sup>	13.06 <sup>a</sup>
			213.7 <sup>b</sup>	12.59 <sup>b</sup>

<sup>a</sup> at  $E_{c.m.} = 230$  MeV.

<sup>b</sup> at  $E_{c.m.} = 300$  MeV.

light and medium mass systems as well as highly mass-asymmetric systems fusion generally occurs immediately above the ion-ion potential barrier, while in heavier systems there is an energy range above the barrier where capture does not occur. The energy difference between

the DC-TDHF potential barrier and the interaction barrier is the extrapush energy introduced by Swiatecki in a macroscopic model [36]; in addition to the work presented here, this phenomenon has recently been studied for heavy and nearly symmetric reaction partners using the TDHF method [37].

### B. Dynamic excitation energy $E^*(R)$

In this subsection, we examine the dynamic excitation energy  $E^*(R(t))$ , computed according to Eq. (4), during the initial stages of the collision. Of particular interest is the excitation energy at the capture point,  $E_c^*$ , which will influence the outcome of the reaction. In Fig. 5 the pre-

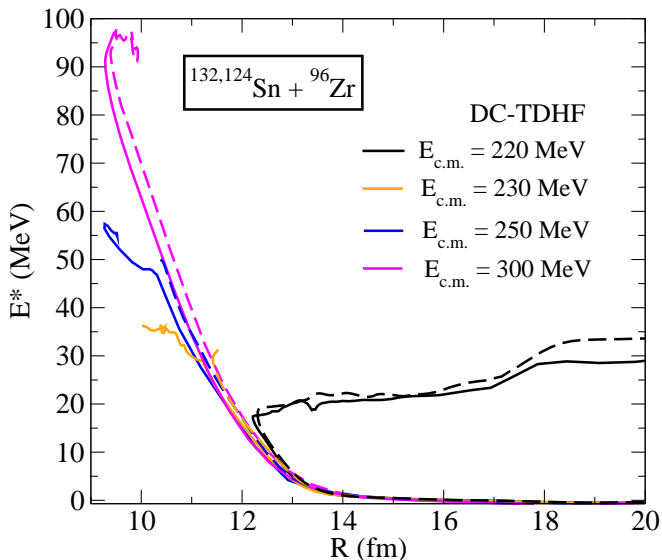


FIG. 5. (color online) Pre-compound excitation energy as a function of the internuclear distance  $R$ , calculated at zero impact parameter with the DC-TDHF method at four  $E_{c.m.}$  energies. Compared are the neutron-rich system  $^{132}\text{Sn} + ^{96}\text{Zr}$  (solid lines) and the stable system  $^{124}\text{Sn} + ^{96}\text{Zr}$  (dashed lines).

compound excitation energies are shown as a function of the internuclear distance  $R$ ; this represents our first microscopic calculation for neutron-rich systems. When the two nuclei are far apart, the excitation energy is zero (this provides a good test for the numerical accuracy of the DC-TDHF calculation). As the two ions approach each other the excitation energy increases rapidly and reaches values between 30 - 90 MeV for the given range of c.m. energies. It is interesting to note that at  $E_{c.m.} = 220$  MeV TDHF theory predicts that the two ions bounce back despite the fact that they are almost 10 MeV above the corresponding potential barrier, i.e. at this energy we have predominantly deep-inelastic reactions rather than capture. This is due to the fact that a large part of the incoming c.m. energy was converted to internal excitation  $E^*$  such that the collective energy does not suffice any more to surmount the barrier. This feature was also

shown in the figure for the corresponding heavy-ion interaction potential (dotted line in Fig. 3).

In Fig. 6 we show the excitation energy  $E_c^*$  at the capture point as a function of  $E_{c.m.}$ . The capture point is defined as the distance  $R$  inside the barrier region where the collective kinetic energy, Eq. (6), becomes zero. Because

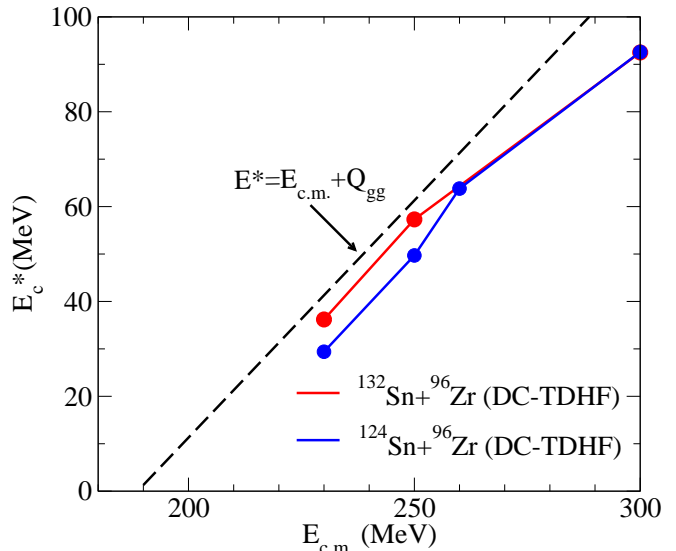


FIG. 6. (color online) Pre-compound excitation energy at the capture point,  $E_c^*$ , as function of the c.m. energy, as predicted by DC-TDHF for a central collision.

of the very elongated shape of the dinuclear composite system at the capture point,  $E_c^*$  is systematically lower than one would expect for the compound nuclei  $^{228,220}\text{Th}$  in their ground state (dashed line in Fig. 6)

$$E^* = E_{c.m.} + Q_{gg} . \quad (10)$$

The last expression can be derived from reaction kinematics. The  $Q$ -values are obtained from measured binding energies of the reaction partners and the compound nuclei. For the two systems considered here the  $Q$ -values are almost identical:  $Q_{gg} = -188.7$  MeV for  $^{132}\text{Sn} + ^{96}\text{Zr}$  and  $Q_{gg} = -188.4$  MeV for  $^{124}\text{Sn} + ^{96}\text{Zr}$ , hence we have drawn only one curve for both systems (dashed line in Fig. 6). We observe that the excitation energy  $E_c^*$  at the capture point is somewhat lower for the  $^{124}\text{Sn} + ^{96}\text{Zr}$  system in the energy range  $E_{c.m.} = 230 - 250$  MeV; at higher  $E_{c.m.}$  energies, their excitation energies are almost identical. In this context, we would like to mention that recent microscopic calculations [38] have shown that the temperature (excitation energy) of the actinide compound nuclei will strongly influence the height of their fission barriers.

### C. Capture and deep-inelastic cross section for $^{132}\text{Sn} + ^{96}\text{Zr}$

Previously, we have studied heavy-ion fusion of the neutron-rich system  $^{132}\text{Sn} + ^{64}\text{Ni}$  using the DC-TDHF



method [21, 22]. In that case, the fission barrier of the compound system is so high that the fission contribution is negligible at energies near the Coulomb barrier. By contrast, the compound nuclei for the systems studied in the present paper,  $^{132,124}\text{Sn}+^{96}\text{Zr}$ , are the actinides  $^{228,220}\text{Th}$  with a fission barrier of only about 6 MeV. We therefore expect sizable fission competition, and the evaporation residue cross section will be quite small. Depending upon beam energy and impact parameter, the dominant reaction channels are deep-inelastic and capture reactions. In general, central collisions and collisions with relatively small impact parameter result in capture (one fragment in the exit channel), while at larger impact parameters the system tends to disintegrate into two fragments after some mass and charge transfer (deep-inelastic reactions). Regarding the capture channel, the composite system will eventually decay by nucleon and photon emission or by fission. This long-time evolution of the composite system is beyond the scope of TDHF due to the absence of quantum decay processes and transitions. In Fig. 7 we show total capture and deep-inelastic cross sections for the neutron-rich system  $^{132}\text{Sn}+^{96}\text{Zr}$ . Let us first discuss the results obtained with the DC-

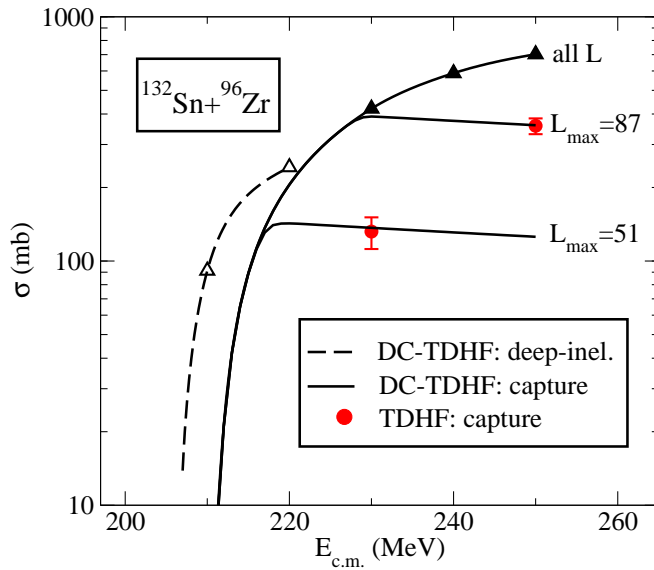


FIG. 7. (color online) Total cross section for capture (solid line) and for deep-inelastic reactions (dashed line) for the neutron-rich system  $^{132}\text{Sn}+^{96}\text{Zr}$  calculated with the DC-TDHF method as function of  $E_{c.m.}$ . Total capture cross sections predicted by unrestricted TDHF calculations are also given (red dots with error bars). For details, see the text.

TDHF method, which can be used at energies  $E_{c.m.}$  below and above the potential barriers. From a comparison of the heavy-ion potentials in Fig. 4 with the nuclear density distributions at the distance of closest approach, see Fig. 1, we conclude that only potentials calculated at energies  $E_{c.m.} \geq 230$  MeV lead to a true composite system with overlapping cores, i.e. a capture reaction. By contrast, the heavy-ion potentials calculated at ener-

gies  $E_{c.m.} < 230$  MeV correspond to a dinuclear system where both nuclei maintain separate cores, i.e. deep-inelastic reactions. The DC-TDHF capture cross section at  $E_{c.m.} = 230$  MeV has been calculated from the energy-dependent heavy-ion potential at 230 MeV. Similar calculations were carried out at energies  $E_{c.m.} = 240$  and 250 MeV. These capture cross sections are marked by filled triangles, and the solid line represents an interpolation between the data points. No restrictions were applied to the sum of partial waves  $L$  in Eq. (3), and this curve is therefore marked “all  $L$ ”. The capture cross sections at energies below 230 MeV were obtained from the heavy-ion potential at 230 MeV because this is the lowest potential barrier that leads to capture. The deep-inelastic cross section at  $E_{c.m.} = 220$  MeV was calculated using the energy-dependent heavy-ion potential at 220 MeV. A similar calculation was carried out at energy  $E_{c.m.} = 210$  MeV. These deep-inelastic cross sections are marked by open triangles, and the dashed line represents an interpolation between these data points. The capture cross sections at energies below 210 MeV were calculated from the heavy-ion potential at 210 MeV because this is the lowest potential barrier predicted by DC-TDHF.

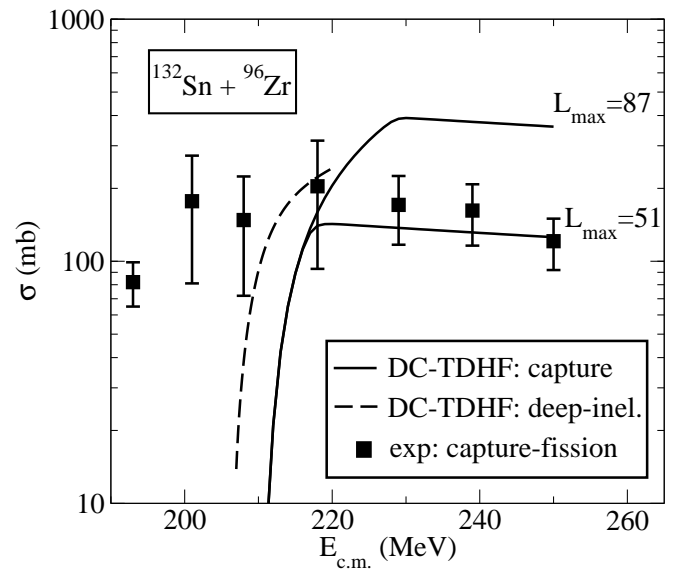


FIG. 8. Total cross section for capture (solid line) and for deep-inelastic reactions (dashed line) for the neutron-rich system  $^{132}\text{Sn}+^{96}\text{Zr}$  calculated with the DC-TDHF method as function of  $E_{c.m.}$ . The experimental capture-fission cross sections are taken from Ref. [3].

At energies above the potential barriers (no barrier tunneling), we have also carried out unrestricted TDHF runs with impact parameters in the range of 0 – 4 fm. By examining the density contours as a function of time, one can easily distinguish between capture events (one fragment in the exit channel) and deep-inelastic reactions (two fragments). At  $E_{c.m.} = 250$  MeV we find that impact parameters  $b = 0 - 3.25$  fm result in capture, while impact parameters  $b \geq 3.50$  fm lead to deep-

inelastic reactions. Using the sharp cut-off model, the capture cross section is given by  $\sigma_{\text{capt}} = \pi b_{\text{max}}^2$  with  $b_{\text{max}} = 3.375 \pm 0.125$  fm. This cross section is shown by a red dot in Fig. 7, with the corresponding theoretical error bar arising from the impact parameter spacing. The impact parameter  $b_{\text{max}} = 3.375$  fm corresponds to an orbital angular momentum quantum number  $L_{\text{max}} = 87$ . If we use this angular momentum cut-off in the IWBC method, we obtain the curve labeled  $L_{\text{max}} = 87$ ; as we can see, both methods yield the same capture cross section. We have carried out a similar calculation at  $E_{\text{c.m.}} = 230$  MeV which yields  $b_{\text{max}} = 2.05 \pm 0.15$  fm and  $L_{\text{max}} = 51$ . The corresponding TDHF and DC-TDHF capture cross sections are also plotted in Fig. 7.

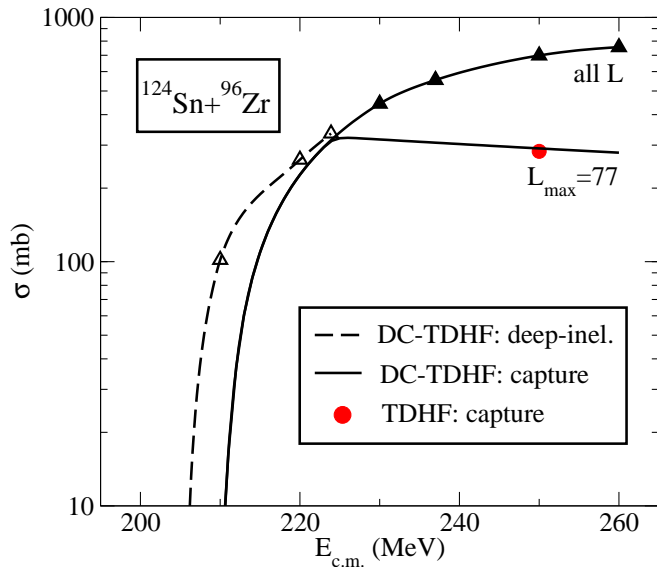


FIG. 9. (color online) Total cross section for capture (solid line) and for deep-inelastic reactions (dashed line) for the stable system  $^{124}\text{Sn} + ^{96}\text{Zr}$  calculated with the DC-TDHF method as function of  $E_{\text{c.m.}}$ . The red dot represents the total capture cross section at  $E_{\text{c.m.}} = 250$  MeV predicted by an unrestricted TDHF run. For details, see text.

In Fig. 8 we compare the DC-TDHF cross sections for deep-inelastic and capture reactions to experimental capture-fission cross sections measured at HRIBF with a radioactive  $^{132}\text{Sn}$  beam [3]. Because the fission probability  $P_{\text{fiss}} \leq 1$ , our *calculated capture cross sections* should be regarded as an *upper limit* for the measured capture-fission cross sections. According to our unrestricted TDHF calculations, the dominant reaction channels at energies  $E_{\text{c.m.}} < 230$  MeV are the deep-inelastic and quasi-elastic channels. In fact, our density plots in Fig. 1 reveal that at the lowest measured energy  $E_{\text{c.m.}} = 195$  MeV the nuclear surfaces barely touch. Any fission from such an event would have to arise from sub-barrier neutron-transfer and should be negligible compared to capture fission at higher energies. We therefore make the conjecture that the bulk of the low-energy experimental data in Fig. 8 represent

deep-inelastic and quasi-elastic events masquerading as capture-fission. Indeed, because of the limited mass resolution in the HRIBF experiments [3] it has been difficult to separate the DIC component from capture-fission. Further experiments with an improved fission fragment detector are planned [39].

#### D. Capture and deep-inelastic cross section for $^{124}\text{Sn} + ^{96}\text{Zr}$

In Fig. 9 we examine the properties of the stable system  $^{124}\text{Sn} + ^{96}\text{Zr}$ . Plotted are total cross sections for capture and for deep-inelastic reactions calculated with the DC-TDHF method as function of the c.m. energy. Like in the corresponding neutron-rich system, only the heavy-ion potentials calculated at energies  $E_{\text{c.m.}} \geq 230$  MeV lead to capture while potentials at lower energies are associated with deep-inelastic channels. We have also carried out unrestricted TDHF runs for this system at  $E_{\text{c.m.}} = 250$  MeV. At impact parameter  $b = 3.5$  fm we find a deep-inelastic reaction, and at  $b = 3.0$  fm we obtain capture. Again, using the sharp cut-off model with  $b_{\text{max}} = 3.0$  fm we obtain the cross section shown by a red dot in Fig. 9. This impact parameter corresponds to an orbital angular momentum quantum number  $L_{\text{max}} = 77$ . If we use this angular momentum cut-off in the DC-TDHF method, we obtain the curve labeled  $L_{\text{max}} = 77$ ; as we can see, both methods yield the same capture cross section.

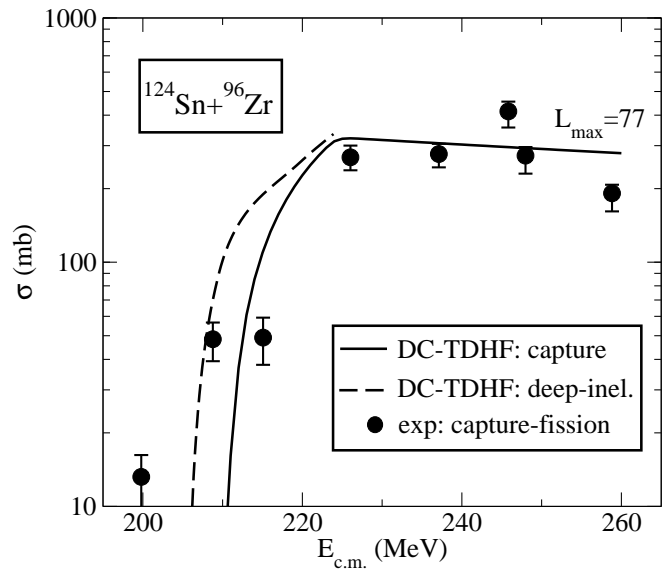


FIG. 10. Total cross section for capture (solid line) and for deep-inelastic reactions (dashed line) for the stable system  $^{124}\text{Sn} + ^{96}\text{Zr}$  calculated with the DC-TDHF method as function of  $E_{\text{c.m.}}$ . The experimental capture-fission cross sections are taken from Ref. [3].

In Fig. 10 we compare the DC-TDHF cross sections for deep-inelastic and capture reactions to experimental capture-fission cross sections measured at HRIBF. Again,



our calculated capture cross sections represent an upper limit for the measured capture-fission data. The agreement between theory and experiment is quite remarkable in view of the fact that we employ a fully microscopic theory based on a given energy functional, with no adjustable parameters related to the capture process.

#### IV. CONCLUSIONS

In this paper we have studied deep-inelastic and capture reactions for the neutron-rich system  $^{132}\text{Sn}+^{96}\text{Zr}$  at energies in the vicinity of the barrier. This is by far the heaviest neutron-rich system we have investigated using both unrestricted TDHF and DC-TDHF methods. To elucidate any special properties neutron-rich systems might possess, we have compared a number of observables to those of the stable system  $^{124}\text{Sn}+^{96}\text{Zr}$ . The dynamic microscopic calculations are carried out on a 3D Cartesian lattice, and they require a large amount of CPU time, particularly with the added DC method.

A contour plot of the mass density of the dinuclear system shows clearly a transition from two separate cores at lower energies to a shape configuration with overlapping cores or a single-core at energies  $E_{c.m.} \geq 230$  MeV. A study of the dynamic quadrupole moment  $Q_{20}(t)$  shows that even at  $E_{c.m.} = 300$  MeV, the intrinsic quadrupole moment is 3 times larger than that of the deformed compound nucleus  $^{228}\text{Th}$  during the initial stages of the collision. We also calculate the heavy-ion interaction potential  $V(R)$ , and we demonstrate that in these very heavy systems the barrier height and width increase dramatically with increasing beam energy  $E_{c.m.}$ . We find that the potential barriers of the neutron-rich system  $^{132}\text{Sn}+^{96}\text{Zr}$  are systematically 1 – 2 MeV higher than those of the

stable system. By contrast, we observe large differences (9 MeV) in the interaction barriers of the two systems which can be deduced from unrestricted TDHF runs. We then examine the dynamic excitation energy  $E^*(t)$  during the initial stages of the collision and compare it to the expression  $E^* = E_{c.m.} + Q_{gg}$  (deduced from reaction kinematics) which assumes that the combined system is in its ground state. Finally, capture cross sections for the two reactions are analyzed in terms of dynamic effects, and a comparison with recently measured capture-fission data is given.

One of the major open questions in the reactions of neutron-rich nuclei is the dependence of the barrier on isospin  $T_z = (Z - N)/2$ . To reveal possible systematic trends requires additional theoretical and experimental studies with a wide variety of projectile and target combinations which are expected to become available at current and future RIB facilities. To be able to pin down the isospin dependence in a fully microscopic theory, it is probably best to choose collision partners which are as simple as possible: projectile and target nuclei should be spherical in their ground state, and the compound nucleus should have a high fission barrier so that the fission component can be ignored (at least at lower beam energies). A desirable reaction system of this kind appears to be  $^{132}\text{Sn}+^{40,48,54}\text{Ca}$ , and we are planning to investigate these reactions in the future.

#### ACKNOWLEDGMENTS

This work has been supported by the U.S. Department of Energy under Grant No. DE-FG02-96ER40963 with Vanderbilt University, and by the German BMBF under Contracts No. 06F131 and No. 06ER142D.

- 
- [1] J. F. Liang *et al.*, Phys. Rev. Lett. **91**, 152701 (2003); **96**, 029903(E) (2006).
  - [2] J. F. Liang, D. Shapira, C. J. Gross, R. L. Varner, J. R. Beene, P. E. Mueller, and D. W. Stracener, Phys. Rev. C **78**, 047601 (2008).
  - [3] A. M. Vinodkumar *et al.*, Phys. Rev. C **78**, 054608 (2008).
  - [4] S. Hofmann *et al.*, Eur. Phys. J. A **14**, 147 (2002).
  - [5] Yu. Ts. Oganessian *et al.*, Phys. Rev. Lett. **104**, 142502 (2010).
  - [6] T. Ichikawa, A. Iwamoto, P. Möller, and A.J. Sierk, Phys. Rev. C **71**, 044608 (2005).
  - [7] V. Yu. Denisov and W. Nörenberg, Eur. Phys. J. A **15**, 375 (2002).
  - [8] G. Fazio, *et al.*, Eur. Phys. J. A **19**, 89 (2004).
  - [9] A. K. Nasirov, G. Giardina, G. Mandaglio, M. Mangano, F. Hanappe, S. Heinz, S. Hofmann, A. I. Muminov, W. Scheid, Phys. Rev. C **79**, 024606-10 (2009).
  - [10] G. G. Adamian, N. V. Antonenko, and W. Scheid, Eur. Phys. J. A **41**, 235 (2009).
  - [11] J. W. Negele, Rev. Mod. Phys. **54**, 913 (1982).
  - [12] K. T. R. Davies, K. R. Sandhya Devi, S. E. Koonin, and M. R. Strayer, page 3 in “Treatise on Heavy-Ion Physics, Vol. 3 Compound System Phenomena” edited by D. A. Bromley, Plenum Press, New York, 1985.
  - [13] E. Chabanat, P. Bonche, P. Haensel, J. Meyer and R. Schaeffer, Nucl. Phys. **A635**, 231 (1998); **A643**, 441(E) (1998).
  - [14] M. Bender, P.-H. Heenen, and P.-G. Reinhard, Rev. Mod. Phys. **75**, 121 (2003).
  - [15] A. S. Umar and V. E. Oberacker, Phys. Rev. C **73**, 054607 (2006).
  - [16] Lu Guo, J. A. Maruhn, P.-G. Reinhard, and Y. Hashimoto, Phys. Rev. C **77**, 041301(R) (2008).
  - [17] Kouhei Washiyama and Denis Lacroix, Phys. Rev. C **78**, 024610 (2008).
  - [18] David J. Kedziora and Cédric Simenel, Phys. Rev. C **81**, 044613 (2010).
  - [19] Y. M. Engel, D. M. Brink, K. Goeke, S. J. Krieger, and D. Vautherin, Nucl. Phys. A **249**, 215 (1975).
  - [20] A. S. Umar and V. E. Oberacker, Phys. Rev. C **74**, 021601(R) (2006).

- [21] A. S. Umar and V. E. Oberacker, Phys. Rev. C **74**, 061601(R) (2006).
- [22] A. S. Umar and V. E. Oberacker, Phys. Rev. C **76**, 014614 (2007).
- [23] A. S. Umar and V. E. Oberacker, Phys. Rev. C **77**, 064605 (2008).
- [24] A. S. Umar and V. E. Oberacker, Eur. Phys. J. A **39**, 243 (2009).
- [25] A. S. Umar, J. A. Maruhn, N. Itagaki, and V.E. Oberacker, Phys. Rev. Lett. **104**, 212503 (2010).
- [26] A. S. Umar, V. E. Oberacker, J. A. Maruhn, and P.-G. Reinhard, Phys. Rev. C **81** 064607 (2010).
- [27] A. S. Umar and V. E. Oberacker, Phys. Rev. C **74**, 061601(R) (2006).
- [28] G. H. Rawitscher, Phys. Rev. **135**, 605 (1964).
- [29] K. Hagino and Y. Watanabe, Phys. Rev. C **76**, 021601(R) (2007).
- [30] R. Y. Cusson, P.-G. Reinhard, M. R. Strayer, J. A. Maruhn, and W. Greiner, Z. Phys. A **320**, 475 (1985).
- [31] A. S. Umar, V. E. Oberacker, J. A. Maruhn, and P.-G. Reinhard, Phys. Rev. C **80**, 041601(R) (2009).
- [32] A. S. Umar and V. E. Oberacker, J. Phys. G: Nucl. Part. Phys. **36**, 025101 (2009).
- [33] G. R. Satchler and W. G. Love, Phys. Rep. **55**, 183 (1979).
- [34] M. J. Rhoades-Brown, V. E. Oberacker, M. Seiwert, and W. Greiner, Z. Phys. A **310**, 287 (1983).
- [35] G. Bertsch, J. Borysowicz, H. McManus, and W. G. Love, Nucl. Phys. A **284**, 399 (1977).
- [36] W. Swiatecki, Nucl. Phys. A **376**, 275 (1982).
- [37] Cédric Simenel, Benoît Avez, Cédric Golabek, (<http://arxiv.org/abs/0904.2653v1>).
- [38] J. C. Pei, W. Nazarewicz, J. A. Sheikh, and A. K. Kerman, Phys. Rev. Lett. **102**, 192501 (2009).
- [39] D. Shapira, ORNL, private communication.